TITLE PAGE

Title

Predicting incremental and future visual change in neovascular age-related macular degeneration using deep learning

Author listing

Dun Jack Fu[1*], Livia Faes[1,2*], Siegfried K. Wagner[1], Gabriella Moraes[1], Reena Chopra[1], Praveen J. Patel, Konstantinos Balaskas[1], Tiarnan D. L. Keenan[3], Lucas M. Bachmann[4], Pearse A. Keane[1]

* Equal contributors

Institutions

[1] NIHR Biomedical Research Centre At Moorfields Eye Hospital NHS Foundation Trust, UCL Institute of Ophthalmology, London, UK

[2] Eye Clinic of the Cantonal Hospital of Lucerne, Lucerne, Switzerland

[3] Division of Epidemiology and Clinical Applications, National Eye Institute, National Institutes of Health, Bethesda, Maryland, USA

[4] Medignition Inc Healthcare Innovations, Zurich, Switzerland

Financial support

This study was sponsored by Moorfields Eye Hospital NHS Foundation Trust. No specific funding was provided for the study. The sponsor was involved in the design and conduct of the study but now with subsequent collection, management, analysis, and interpretation of data; not with preparation, review, or approval of the manuscript; and not with the decision to submit the manuscript for publication.

Conflicts of interest

Dr Keane has received speaker fees from Heidelberg Engineering, Topcon, Carl Zeiss Meditec, Haag-Streit, Allergan, Novartis, and Bayer. He has served on advisory boards for Novartis and Bayer and has been an external consultant for DeepMind and Optos. Dr Faes reports other relevant financial activities outside the submitted work with Bayer, and Allergan. Dr Keenan has received grant funding from Bayer (Global Ophthalmology Award Program awardee) through NEI. Dr Balaskas has received speaker fees from Novartis, Bayer, Alimera, Allergan and research support from Novartis and Bayer. Dr Patel has received lecturing, educational travel, advisory board fees for Bayer UK, Novartis UK, and Roche UK.
All other authors report no conflicts of interest.

Corresponding author

Pearse A. Keane
162 City Rd, London EC1V 2PD
+44 (0) 2072533411
pearse.keane1@nhs.net

ABSTRACT

Purpose: To evaluate the predictive utility of quantitative imaging biomarkers, acquired automatically from optical coherence tomography (OCT) scans, of cross-sectional and future visual outcomes of patients with neovascular age-related macular degeneration (AMD) starting anti-vascular endothelial growth factor (VEGF) therapy.

Design: Retrospective cohort study.

Participants: Treatment-naïve, first-treated eyes of patients with neovascular AMD between 2007 and 2017 at Moorfields Eye Hospital (a large, UK single-centre) undergoing anti-VEGF therapy

Methods:
Automatic segmentation was carried out by applying a deep learning segmentation algorithm to 137,379 OCT scans from 6467 eyes of 3261 patients with neovascular AMD. After applying selection criteria 926 eyes of 926 patients were taken forward for analysis.

Main outcome measures: Correlation coefficients (R^2) and mean absolute error (MAE) between quantitative OCT (qOCT) parameters and cross-sectional visual-function. The predictive value of these parameters for short-term visual change i.e. incremental visual acuity [VA] resulting from an individual injection, as well as, VA at distant timepoints (up to 12 months post-baseline).

Results:
VA at distant timepoints could be predicted: R^2 0.79 (MAE 5.0 ETDRS letters) and R^2 0.63 (MAE 7.2) post-injection 3 and at 12 months post-baseline (both $p < 0.001$), respectively. Best performing models included both baseline qOCT parameters and treatment-response. Furthermore, we present proof-of-principle evidence that the incremental change in VA from an injection can be predicted: R^2 0.13 (MAE 5.6) for injection 2 and R^2 0.07 (MAE 5.0) for injection 3 (both $p < 0.01$).

Conclusions:
Automatic segmentation enables rapid acquisition of quantitative and reproducible OCT biomarkers with potential to inform treatment decisions in the care of neovascular AMD. This furthers development of point-of-care decision-aid systems for personalized medicine.

INTRODUCTION

Neovascular age-related macular degeneration (AMD) is a leading cause of central vision loss in the developed world,[1,2] but its visual prognosis can be substantially improved with anti-angiogenic treatment.[3-4] Treatment regimens have generally evolved from fixed monthly injections to more proactive protocols that balance treatment burden against efficacy - the most commonly adopted being the “treat-and-extend” regimen.[5-6] Here, treatment intervals are informed by presence of exudative disease activity, determined by regular, qualitative assessment of optical coherence tomography (OCT) imaging specific anatomical biomarkers, as recommended by ophthalmology bodies.[7–9] Large-scale studies have demonstrated that manual, qualitative characterisation of retinal structures (such as intraretinal fluid [IRF], subretinal fluid [SRF] and pigment epithelial detachment [PED]) correlate with treatment response.[10,11] Manual efforts on small cohorts have shown that further characterisation of these variables - segmenting and quantifying the volume (i.e. transforming the variable from categorical to continuous) - confers greater predictive value.[12] However, manual characterisation of these features, even in a qualitative way (i.e. the binary assessment of presence or absence), is time-consuming and prone to substantial inter-grader variability.[13] This exposes clinical decisions to variation that is likely unwanted in both real-world care and clinical trial settings.[14,15]

A promising advance is the use of artificial intelligence to develop algorithms that automatically process volumetric OCT scans of the retina, quantifying each of its anatomical constituents in three-dimensions thus providing quantitative OCT (qOCT) parameters.[16–18] Although not yet established in clinical practice, automatic qOCT generates rapidly-accessible, objective data and is thus ideally suited to identifying and evaluating the utility of anatomical biomarkers for *diagnosis* and *prognosis*. That is, key disadvantages of manual segmentation are overcome: potential measurement bias, examiner variability and the inherently labour-intensive process that limits both study sample size and clinical applicability.

In this study, we apply a deep learning segmentation algorithm to a real-world dataset comprising 137,379 OCT scans of 6467 unique eyes (3261 patients) with neovascular AMD undergoing anti-VEGF therapy. The prognostic value of the qOCT biomarkers for disease activity and treatment-response was evaluated to explore their utility for individualized patient injection schedules. Moreover, our dataset and analyses will be deidentified and made available through an open-source digital repository to enable independent replication of our results and permit follow-up analyses by other research groups.

METHODS

Study design, setting and cohort selection

This study was designed as a post hoc analysis of real-world data obtained prospectively during the clinical care of patients with the Moorfields Eye Hospital (MEH) AMD database. MEH is a tertiary referral center for eye diseases in the United Kingdom and maintains an OCT database of routinely collected data from patients with neovascular AMD that started anti-angiogenic therapy between 2007 and 2017. The database consists of demographic (age, gender and ethnicity) and clinical features. Selection criteria, patient demographics and clinical characteristics of 8174 eyes of 6664 patients with 120,756 treatment episodes from this database has been reported by Fasler and colleagues in 2018.[19] Each treatment episode is associated with at least one retinal OCT scan (and, in the case of duplicate scans, the one with fewer artefacts was included).

Here we selected all first-treated eyes of the MEH AMD dataset that had completed the induction phase of anti-VEGF therapy appropriately (i.e. received the first 3 injections with intervals between each injection shorter than 60 days) and had VA and injection data recorded at each visit within the induction phase. In cases of simultaneously treated eyes, one was selected randomly. If OCT data were missing at baseline, scans acquired within 14 days prior to the baseline were used instead. Patients were started on a modified treat-and-extend regimen[19] with either aflibercept (828 patients; 89%) or ranibizumab (98 patients; 11%) This research project was conducted in accordance with the research protocol and the Declaration of Helsinki.[20,21]

Datasource

This study utilises a deep learning model to segment retinal layers and fluid from OCT scans.[17] The segmentation deep learning model classified each voxel as either: epiretinal membrane, neurosensory retina, retinal pigment epithelium (RPE), drusenoid pigment epithelium detachment (PED), serous PED, fibrovascular PED, SRF, IRF, subretinal hyperreflective material (SHRM), hyperreflective foci (HRF), choroid and beyond, vitreous and subhyaloid space, posterior hyaloid, or artefacts. Serous PED, fibrovascular PED and drusenoid PED were summed and considered as a collective feature - PED. Each of these retinal structures was extrapolated from 6x6 mm 3DOCT-2000 (Topcon Corp., Tokyo, Japan) macula-centered OCT scans into quantitative (qOCT) values, which were presented as volumetric measurements in mm^3 or µl. This has been previously detailed [Moraes *et al.* Manuscript under review]. Briefly, the segmenting deep learning algorithm extracts voxels that each correspond to a volume of 2.60 µm (A-scan) x 11.72 µm (B-scan) x 47.24 µm (C-scan direction). An example of a B-scan segmentation is depicted in **Figure 1a**.

Prediction of visual outcomes

Qualitative studies have reported associations between retinal structures and disease activity in AMD.[12,22,23] Based on these publications, the following structures featured in our automatic segmentation algorithm were selected as candidate qOCT biomarkers: RPE, IRF, SRF, PED, SHRM and HRF. They were each considered as independent variables for three distinct VA outcomes as dependent variables (**Figure 1b**): (i) the relationship between qOCT biomarkers and VA acquired at the same

timepoint (e.g. volume of RPE at month 12 and VA at month 12). This cross-sectional correlation effectively evaluates the association between retinal structure and visual function at the same point in time. timepoints considered were baseline (immediately prior to starting anti-VEGF therapy), post-injection 1, post-injection 2, post-injection 3 and 12 months after baseline. (ii) The predictive value of qOCT biomarkers for VA at future timepoints: post-injection 2, post-injection 3 and 12 months post-baseline. (iii) The incremental change in VA following the second or third injections.

Injections 1, 2 and 3 were given at baseline, 1 month post-baseline and 2 months post-baseline, respectively. Resultant VAs were measured 30 to 60 days afterwards i.e. just prior to the subsequent injection. Incremental change was calculated by subtracting pre-injection VA from resultant VA, i.e. $\mathbf{VA_{[month\ 2]} - VA_{[month\ 1]}}$ for the second injection and $\mathbf{VA_{[month\ 3]} - VA_{[month\ 2]}}$ for the third. For visual outcomes (ii) and (iii), additional independent variables capturing treatment-response to previous injections were also considered. These were the incremental visual (VA) and morphometric (qOCT biomarkers) changes resulting from each of the preceding induction injections. For instance, treatment-response to injection 2 was included as $\mathbf{VA_{[month\ 2]} - VA_{[month\ 1]}}$ and $\mathbf{qOCT\ biomarker_{[month\ 2]} - qOCT\ biomarker_{[month\ 1]}}$ (e.g. $\mathbf{IRF_{[month\ 2]} - IRF_{[month\ 1]}}$).

Each of the visual outcomes above was considered as a continuous dependent variable, wherein the coefficient of determination (R^2) was computed by ordinary least squares regression and was reported from 100-fold bootstrapped models. For visual outcome (ii), binomial non-linear logistic regression was also used to model the VA $\geq$ 70 and $\leq$ 35 ETDRS letter thresholds at the timepoint following injection 3 and at 12 months post-baseline. Performance was reported using 2-fold cross-validated AUC estimates. These were multivariable regressions including each of the qOCT biomarkers and VA. Notably, demographic data were not included.

Statistical analysis

All data analyses were carried out using R (https://www.r-project.org/) provided in the public domain by R Core team 2020 R Foundation for Statistical Computing, Vienna, Austria.[24] Statistically and clinically significant methods were identified as grouping variables for each visual outcome. Calculated means in text and figures are expressed with ± error standard deviation, unless otherwise specified. P-values < 0.05 were considered significant.

Data sharing statement

A deidentified version of our dataset and its analysis in step-by-step R code will be made available in an open-source digital repository to permit transparency and replication of our results. Data available from the Dryad Digital Repository: https://doi.org/10.5061/dryad.573n5tb5d

RESULTS

Study cohort demography

The study cohort comprised 926 treatment-naive eyes (of 926 patients) that received the three initial anti-VEGF injections of the induction period and were followed up at 12 months (study flow depicted in **Supplementary Figure 1**). Mean age at treatment initiation was 78.9 ± 8.68 years and the majority were female (541; 58.4%) and Caucasian (492; 53.1%) (**Table 1a**).

Cross-sectional structure-function correlation between retinal tissue volumes and visual acuity

Visual acuity data in the form of ETDRS letters and OCT scans were recorded at baseline (timepoint immediately prior to first injection), post-injection 1, post-injection 2, post-injection 3 and 12 months post-baseline for all patients (**Figure 2, Supplementary Table 1a**). From a total of 4630 OCT scans, the volumes of retinal layers (IRF, SRF, PED, SHRM, HRF and RPE) were automatically acquired as morphometric qOCT parameters. As expected, the largest increase in mean VA was observed following the first injection, with smaller changes seen after each subsequent injection. Similarly, the greatest morphometric changes were observed following the first injection, with smaller subsequent changes.

For each timepoint, a cross-sectional correlation was performed between all variables, including the qOCT biomarkers and VA. For all timepoints, significant correlations were observed between the biomarkers and VA (R^2 = 0.11 to 0.17 with mean absolute error [MAE] of 11.0 to 11.9 ETDRS letters, $p < 0.001$; **Table 2**). The qOCT biomarkers demonstrating the most consistently negative correlations were SHRM and IRF (**Supplementary Table 2**). At baseline, every 7.0 ± 0.8 mm^3 ($p < 0.001$) of SHRM and 12.6 ± 1.7 mm^3 ($p < 0.001$) of IRF predicted one fewer ETDRS letter. Conversely, RPE volume was the variable with the most consistent positive correlation (**Supplementary Table 2**). At baseline, each additional RPE volume increase of 33.9 ± 6.7 mm^3 ($p < 0.001$) was associated with one more ETDRS letter. These results indicate that automatically obtained qOCT data can represent some of the morphometric parameters underlying visual function prior to and at any given point during treatment.

Predictive baseline and treatment-response parameters of visual outcome

We next evaluated the potential of qOCT parameters to predict future visual outcomes, namely VA post-injection 2, post-injection 3 and at 12 months post-baseline (considered separately). Baseline qOCT parameters alone were able to predict future VA with R^2 accuracy of 0.15 (MAE 14.1 letters), 0.16 (MAE 14.1 letters) and 0.14 (MAE 12.1 letters) for VA post-injection 2, post-injection 3 and at 12 months post-baseline, respectively (**Table 3**). Predictive accuracy increased markedly following the addition of baseline VA as an independent covariate. Also, predictive accuracy was greater in models with both baseline qOCT parameters and VA(R^2 0.53 [MAE 8.0 letters], 0.49 [MAE 8.4] and 0.36 [MAE 9.9], respectively) than models with baseline VA alone (R^2 0.52 [MAE 8.0 letters], 0.47 [MAE 8.5] and 0.34 [MAE 10.2], respectively). Critically, the greatest accuracies were attained (R^2 0.72 [MAE 5.5 letters], 0.79 [MAE 5.0] and 0.63 [MAE 7.2], respectively) when the predictive models also included previous treatment-response, i.e. incremental changes in VA and qOCT parameters resulting from each of

the previous induction injections. For predicting VA post-injection 2 and 3, the most predictive variable was baseline VA, followed by incremental VA changes from preceding treatment (**Supplementary Table 3**). The most predictive variables of the qOCT biomarkers were RPE, IRF and SHRM.

We next assessed the value of these parameters in predicting clinically significant VA thresholds (VA $\geq$ 70 and VA $\leq$ 35 ETDRS letters) following injection 3 and at 12 months post-baseline. A regression model based on baseline qOCT biomarkers only reached an AUC of 0.69 (95% CI 0.64 - 0.74) in predicting VA $\geq$ 70 and of 0.68 (95% CI 0.58 - 0.79) in predicting VA $\leq$ 35 post-injection 3 (**Figure 3a**). Predictive performance for both tasks increased with the addition of baseline VA (VA $\geq$ 70: AUC 0.84 [95% CI 0.80 - 0.87]; VA $\leq$ 35: AUC 0.79 [95% CI 0.71 - 0.88]). Highest predictive performance was achieved when incorporating visual and morphometric responses to each of the preceding anti-VEGF injections (VA $\geq$ 70: AUC 0.93 [95% CI 0.90 - 0.95]; VA $\leq$ 35: AUC 0.90 [95% CI 0.83 - 0.96]. A similar trend was observed when modelling VA at month 12 (VA $\geq$ 70: AUC 0.87 [95% CI 0.84 - 0.91]; VA $\leq$ 35: AUC 0.86 [95% CI 0.80 - 0.92] (**Figure 3b**).

Prediction of incremental VA change resulting from treatment

Given that future VA outcomes during anti-VEGF therapy can be predicted, we also interrogated whether the incremental VA change resulting from a single anti-VEGF injection could also be modelled. Injections 2 and 3 were selected for the following two reasons. Although the observed mean incremental changes following injections 2 and 3 were low (2.2 ± 8.4 letters and 0.2 ± 7.4 letters, respectively; **Table 1b**), the distribution of incremental VA changes was wide, non-normal (**Figure 2c**; Shapiro-Wilk test $p < 0.001$) and featured clinically relevant changes ($\geq$ 5 letters)[25,26] in more than 38% of cases (**Table 1b**). Second, standardisation of the induction injection regimen allows injection-number and -interval variability to be controlled for at these timepoints.

Baseline parameters alone were not predictive of the incremental VA change following injections 2 and 3 (**Table 4**). However, inclusion of baseline VA and treatment-response to preceding injections yielded greater predictive accuracy and statistical significance (post-injection 2: R^2 0.13 MAE 5.6 letters; post-injection 3: R^2 0.07 MAE 5.0 letters), albeit with overall low performance (**Table 4**). VA responses to previous injections were more predictive than baseline VA (**Supplementary Table 3**). Similarly, morphometric responses following the most recent anti-VEGF injections (namely SHRM, IRF and RPE) were more important features than the baseline values.

DISCUSSION

Main findings

Our data suggest that short- and long-term visual outcomes in patients with neovascular AMD under anti-angiogenic therapy can be predicted using retinal tissue volumes that have been automatically segmented and quantified from OCT imaging. Using baseline VA and qOCT values alone, over forty percent of visual outcome variance at future timepoints can be predicted. Markedly greater accuracy was achieved in models that included functional and anatomical changes following each of the preceding induction injections. Our results therefore suggest that treatment-response is itself predictive of visual outcomes, which is consistent with previous studies.[27–29] Several qOCT biomarkers were identified as statistically significant predictive variables. As such, automatic OCT segmentation may play a role in evaluating disease activity and capacity for treatment-response at the individual injection and patient level.

Results in the context of the existing literature

The defining feature in neovascular AMD is development of macular neovascularization (MNV), accompanied by the exudation of fluid within and beneath the retina. Presence of IRF has itself been identified as a key biomarker of disease activity and poor visual outcomes.[10,12,30–32] Our analyses identify IRF volume as a strong risk factor for low VA. Reduction of IRF from previous anti-VEGF treatments was also predictive of VA increase from future injections. The volume of IRF however, was not predictive of visual function at month 12, which contrasts with reports from Schmidt-Erfurth and colleagues on a separate segmentation algorithm.[33] This discrepancy likely arises from differences in study cohort and design. Our cohort was from real-world clinical practice, where patients were undergoing a treat-and-extend regimen, whereas Schmidt-Erfurth *et al.* (2018) reported on a trial cohort receiving either a fixed monthly or a *pro re nata* dose regimen. The variable injection intervals and the non-refracted VA measurements may have introduced additional noise into our data.

Another potential reason for observed differences is that we considered additional biomarkers - RPE, SHRM or HRF volumes. The identification of these prominent qOCT biomarkers has clear clinical implications: starting treatment at earlier or milder stages - with less IRF, less SHRM and more preserved RPE confers downstream functional benefit.

In patients with neovascular AMD undergoing anti-VEGF therapy, VA deterioration due to RPE degeneration may occur by natural progression independent of MNV, exudation- associated RPE damage and/or controversially, by any contribution from anti-VEGF.[34 35–37] SHRM implies type 2 MNV with potential to develop into a fibrous scar and its presence has been associated with reduced VA and poor anti-VEGF response.[38–40] It is therefore unsurprising that our analyses identified SHRM volume at baseline as a risk factor for poor VA (1 fewer ETDRS letter for every 1.6 ± 1.1 mm^3 of SHRM) and its resolution as a protective factor (1 letter increase for every 3.9 ± 1.9 mm^3 reduction after injection 1) for VA at 12 months.

The relationship between central visual function and structural markers of retinal disease can be affected by their proximity to the fovea. Schmidt-Erfurth and colleagues extrapolated features from within 1 mm of the fovea as opposed to 6 mm carried out in this study. It has been demonstrated that the correlation between cross-sectional VA

and manually-segmented IRF volume can be increased by weighting the volume by distance from the fovea. Going forward, this principle ought to be implemented when evaluating the correlation of qOCT parameters with visual function.

Limitations

This study considers several retinal structures in disease prognosis. However, other important structures with known relevance for disease activity and visual outcome, such as the ellipsoid zone or the external limiting membrane were not considered due to unavailable segmentation data.[30,31,41] Non-retinal structures that are important for vision were not considered either, such as lens or corneal status.

Implications for further research and practice

Determining the optimal dosing schedule of intravitreal injections for the individual patient is a critical step towards delivering personalised care in anti-VEGF therapy. While treat-and-extend and other flexible regimens can be seen as a first step in balancing treatment burden and patients outcomes, unnecessary visits/injections and unintended variation in care are still common and can lead to non-adherence, increased healthcare cost and strains on the healthcare system - ultimately leading to negative consequences on visual outcomes.[42, 43] General guidance on follow-up and investigations of neovascular AMD by professional national and international societies exist,[7–9] however, current treatment protocols feature limited management options that do not sufficiently reflect the diverse responses exhibited by patients with neovascular AMD undergoing anti-angiogenic treatment.[44] Automatic, reproducible and quantitative identification of diagnostic and prognostic factors could together inform the optimal anti-angiogenic treatment regimen tailored to an eye.

Most studies on prognostic OCT biomarkers focus on long-term visual outcomes, such as using baseline OCT parameters to predict VA at 12 months.[12,33,45] Yet, interestingly, short-term outcome predictions hold separate value and utility. When considering a patient who has had nine injections and may have a tenth, knowing the visual-outcome probabilities that can arise from an additional injection (increase, decrease, or no change) would be impactful. Certainly, the ability to predict the incremental VA change from a single injection would advance clinical decision-making and progress towards personalised treatment regimens.

One approach to build such a decision-aid tool could be through reinforcement learning, a type of artificial intelligence. This novel technique has been successfully applied to various medical problems in recent years, such as diabetes, mechanical ventilation and sepsis management in the intensive care unit.[46–49] Reinforcement learning has several theoretical advantages over existing algorithms, particularly when dealing with a suboptimal gold standard in a sequential decision-making paradigm such as in anti-VEGF therapy.[47,49] In contrast to deep learning models, reinforcement learning is not limited by a supervised regimen and the associated ceiling effect of the current gold standard, i.e. the clinician's decision on the anti-VEGF treatment schedule based on qualitative assessment of OCT biomarkers for disease activity.[14,15] Reinforcement learning has the potential to distinguish optimal from suboptimal clinical decisions, by using a patient's clinical and demographic information and qOCT

biomarkers (model's input) to predict the optimal treatment interval for the individual AMD patient (model's output).

Conclusion

Automatic segmentation potentially enables rapid acquisition of quantitative and reproducible OCT biomarkers that can be used to inform treatment decisions. We present proof-of-principle evidence that incremental change in visual function from a single injection can be predicted. Further research ought to enable point-of-care decision-aid systems that support the clinician to individualize anti-angiogenic therapy and reduce unwanted variation in care for neovascular AMD. Lastly, we make a deidentified version of our data available to enable independent replication to enable follow-up analyses and facilitate further enquiry by other research groups.

ACKNOWLEDGEMENTS

Funding/support: The research supported by the National Institute for Health Research (NIHR) Biomedical Research Centre based at Moorfields Eye Hospital NHS Foundation Trust and UCL Institute of Ophthalmology.

Financial disclosures:
Dr. Keane has received speaker fees from Heidelberg Engineering, Topcon, Carl Zeiss Meditec, Haag-Streit, Allergan, Novartis, and Bayer. He has served on advisory boards for Novartis and Bayer and has been an external consultant for DeepMind and Optos.
Dr. Bachmann is the CEO of Oculocare Inc.
Dr. Patel has received lecturing, educational travel, advisory board fees for Bayer UK and Novartis UK.
Dr. Balaskas has received speaker fees from Novartis, Bayer, Alimera, Allergan and research support from Novartis and Bayer.
RC receives studentship support from the College of Optometrists, UK. Independent of this work, R.C. is also affiliated with Google LLC. Google LLC played no role in this work aside from data released from prior published work.

REFERENCES

1. Bressler, N. M. Age-related macular degeneration is the leading cause of blindness. *JAMA: the journal of the American Medical Association* vol. 291 1900–1901 (2004).
2. Jager, R. D., Mieler, W. F. & Miller, J. W. Age-related macular degeneration. *N. Engl. J. Med.* **358**, 2606–2617 (2008).
3. Rosenfeld, P. J. *et al.* Ranibizumab for neovascular age-related macular degeneration. *N. Engl. J. Med.* **355**, 1419–1431 (2006).
4. Heier, J. S. *et al.* Intravitreal aflibercept (VEGF trap-eye) in wet age-related macular degeneration. *Ophthalmology* **119**, 2537–2548 (2012).
5. Regillo, C. D. *et al.* Randomized, double-masked, sham-controlled trial of ranibizumab for neovascular age-related macular degeneration: PIER Study year 1. *Am. J. Ophthalmol.* **145**, 239–248 (2008).
6. Chin-Yee, D., Eck, T., Fowler, S., Hardi, A. & Apte, R. S. A systematic review of as needed versus treat and extend ranibizumab or bevacizumab treatment regimens for neovascular age-related macular degeneration. *Br. J. Ophthalmol.* **100**, 914–917 (2016).
7. Schmidt-Erfurth, U. *et al.* Guidelines for the management of neovascular age-related macular degeneration by the European Society of Retina Specialists (EURETINA). *Br. J. Ophthalmol.* **98**, 1144–1167 (2014).
8. Overview | Age-related macular degeneration | Guidance | NICE.
9. Age-Related Macular Degeneration PPP 2019. *American Academy of Ophthalmology* https://www.aao.org/preferred-practice-pattern/age-related-macular-degeneration-ppp (2019).
10. Jaffe, G. J. *et al.* Macular Morphology and Visual Acuity in the Comparison of Age-related Macular Degeneration Treatments Trials. *Ophthalmology* vol. 120 1860–1870 (2013).
11. Simader, C. *et al.* Morphologic parameters relevant for visual outcome during anti-angiogenic therapy of neovascular age-related macular degeneration. *Ophthalmology* **121**, 1237–1245 (2014).
12. Waldstein, S. M. *et al.* Correlation of 3-Dimensionally Quantified Intraretinal and Subretinal Fluid With Visual Acuity in Neovascular Age-Related Macular Degeneration. *JAMA Ophthalmol.* **134**, 182–190 (2016).
13. Keenan, T. D. *et al.* Retinal specialist versus artificial intelligence detection of retinal fluid from optical coherence tomography: AREDS2 10-year Follow-On. *Ophthalmology* (2020) doi:10.1016/j.ophtha.2020.06.038.
14. Mehta, H. *et al.* Real-world outcomes in patients with neovascular age-related macular degeneration treated with intravitreal vascular endothelial growth factor inhibitors. *Prog. Retin. Eye Res.* **65**, 127–146 (2018).
15. CATT Research Group *et al.* Ranibizumab and bevacizumab for neovascular age-related macular degeneration. *N. Engl. J. Med.* **364**, 1897–1908 (2011).
16. Schlegl, T., Waldstein, S. M., Vogl, W.-D., Schmidt-Erfurth, U. & Langs, G. Predicting Semantic Descriptions from Medical Images with Convolutional Neural Networks. *Inf. Process. Med. Imaging* **24**, 437–448 (2015).
17. De Fauw, J. *et al.* Clinically applicable deep learning for diagnosis and referral in retinal disease. *Nat. Med.* **24**, 1342–1350 (2018).
18. Schmidt-Erfurth, U., Vogl, W.-D., Jampol, L. M. & Bogunović, H. Application of

automated quantification of fluid volumes to anti-VEGF therapy of neovascular age-related macular degeneration. *Ophthalmology* (2020) doi:10.1016/j.ophtha.2020.03.010.
19. Fasler, K. *et al.* One- and two-year visual outcomes from the Moorfields age-related macular degeneration database: a retrospective cohort study and an open science resource. *BMJ Open* **9**, e027441 (2019).
20. Goodyear, M. D. E., Krleza-Jeric, K. & Lemmens, T. The Declaration of Helsinki. *BMJ* **335**, 624–625 (2007).
21. Moons, K. G. M. *et al.* Transparent Reporting of a multivariable prediction model for Individual Prognosis or Diagnosis (TRIPOD): explanation and elaboration. *Ann. Intern. Med.* **162**, W1–73 (2015).
22. Lai, T.-T., Hsieh, Y.-T., Yang, C.-M., Ho, T.-C. & Yang, C.-H. Biomarkers of optical coherence tomography in evaluating the treatment outcomes of neovascular age-related macular degeneration: a real-world study. *Sci. Rep.* **9**, 529 (2019).
23. Schmidt-Erfurth, U. & Waldstein, S. M. A paradigm shift in imaging biomarkers in neovascular age-related macular degeneration. *Prog. Retin. Eye Res.* **50**, 1–24 (2016).
24. (2020). RStudio: Integrated Development for R. RStudio, PBC, Boston, MA. RStudio: Integrated Development for R. RStudio, PBC, Boston, MA. (2020).
25. Csaky, K. *et al.* Report From the NEI/FDA Endpoints Workshop on Age-Related Macular Degeneration and Inherited Retinal Diseases. *Invest. Ophthalmol. Vis. Sci.* **58**, 3456–3463 (2017).
26. Csaky, K. G., Richman, E. A. & Ferris, F. L., 3rd. Report from the NEI/FDA Ophthalmic Clinical Trial Design and Endpoints Symposium. *Invest. Ophthalmol. Vis. Sci.* **49**, 479–489 (2008).
27. Kaiser, P. K. *et al.* Ranibizumab for predominantly classic neovascular age-related macular degeneration: subgroup analysis of first-year ANCHOR results. *Am. J. Ophthalmol.* **144**, 850–857 (2007).
28. Boyer, D. S. *et al.* Subgroup analysis of the MARINA study of ranibizumab in neovascular age-related macular degeneration. *Ophthalmology* **114**, 246–252 (2007).
29. Bloch, S. B. *et al.* Predictors of 1-year visual outcome in neovascular age-related macular degeneration following intravitreal ranibizumab treatment. *Acta Ophthalmol.* **91**, 42–47 (2013).
30. Sulzbacher, F. *et al.* Correlation of SD-OCT features and retinal sensitivity in neovascular age-related macular degeneration. *Invest. Ophthalmol. Vis. Sci.* **53**, 6448–6455 (2012).
31. Sulzbacher, F. *et al.* Correlation of OCT Characteristics and Retinal Sensitivity in Neovascular Age-Related Macular Degeneration in the Course of Monthly Ranibizumab Treatment. *Investigative Opthalmology & Visual Science* vol. 54 1310 (2013).
32. Ritter, M. *et al.* Intraretinal cysts are the most relevant prognostic biomarker in neovascular age-related macular degeneration independent of the therapeutic strategy. *Br. J. Ophthalmol.* **98**, 1629–1635 (2014).
33. Schmidt-Erfurth, U. *et al.* Machine Learning to Analyze the Prognostic Value of Current Imaging Biomarkers in Neovascular Age-Related Macular Degeneration.

Ophthalmol Retina **2**, 24–30 (2018).
34. Kurihara, T., Westenskow, P. D., Bravo, S., Aguilar, E. & Friedlander, M. Targeted deletion of Vegfa in adult mice induces vision loss. *J. Clin. Invest.* **122**, 4213–4217 (2012).
35. Vander, J. F. Ranibizumab and Bevacizumab for Neovascular Age-Related Macular Degeneration. *Yearbook of Ophthalmology* vol. 2012 145–146 (2012).
36. Chakravarthy, U. *et al.* Alternative treatments to inhibit VEGF in age-related choroidal neovascularisation: 2-year findings of the IVAN randomised controlled trial. *Lancet* **382**, 1258–1267 (2013).
37. Ho, A. C. *et al.* Twenty-four-month efficacy and safety of 0.5 mg or 2.0 mg ranibizumab in patients with subfoveal neovascular age-related macular degeneration. *Ophthalmology* **121**, 2181–2192 (2014).
38. Keane, P. A. *et al.* Evaluation of age-related macular degeneration with optical coherence tomography. *Surv. Ophthalmol.* **57**, 389–414 (2012).
39. Byun, Y. J., Lee, S. J. & Koh, H. J. Predictors of response after intravitreal bevacizumab injection for neovascular age-related macular degeneration. *Jpn. J. Ophthalmol.* **54**, 571–577 (2010).
40. Ristau, T. *et al.* Relationship between visual acuity and spectral domain optical coherence tomography retinal parameters in neovascular age-related macular degeneration. *Ophthalmologica* **231**, 37–44 (2014).
41. Mathew, R., Richardson, M. & Sivaprasad, S. Predictive value of spectral-domain optical coherence tomography features in assessment of visual prognosis in eyes with neovascular age-related macular degeneration treated with ranibizumab. *Am. J. Ophthalmol.* **155**, 720–6, 726.e1 (2013).
42. Writing Committee for the UK Age-Related Macular Degeneration EMR Users Group. The neovascular age-related macular degeneration database: multicenter study of 92 976 ranibizumab injections: report 1: visual acuity. *Ophthalmology* **121**, 1092–1101 (2014).
43. Wennberg, J. E. Understanding geographic variations in health care delivery. *The New England journal of medicine* vol. 340 52–53 (1999).
44. Amoaku, W. M. *et al.* Defining response to anti-VEGF therapies in neovascular AMD. *Eye* **29**, 1397–1398 (2015).
45. Schlegl, T. *et al.* Fully Automated Detection and Quantification of Macular Fluid in OCT Using Deep Learning. *Ophthalmology* **125**, 549–558 (2018).
46. Lowery, C. & Faisal, A. A. Towards efficient, personalized anesthesia using continuous reinforcement learning for propofol infusion control. in *2013 6th International IEEE/EMBS Conference on Neural Engineering (NER)* 1414–1417 (2013). doi:10.1109/NER.2013.6696208.
47. Prasad, N., Cheng, L.-F., Chivers, C., Draugelis, M. & Engelhardt, B. E. A Reinforcement Learning Approach to Weaning of Mechanical Ventilation in Intensive Care Units. *arXiv [cs.AI]* (2017).
48. Bothe, M. K. *et al.* The use of reinforcement learning algorithms to meet the challenges of an artificial pancreas. *Expert Rev. Med. Devices* **10**, 661–673 (2013).
49. Komorowski, M., Celi, L. A., Badawi, O., Gordon, A. C. & Faisal, A. A. The Artificial Intelligence Clinician learns optimal treatment strategies for sepsis in intensive care. *Nat. Med.* **24**, 1716–1720 (2018).

50. Reich, O., Schmid, M. K., Rapold, R., Bachmann, L. M. & Blozik, E. Injections frequency and health care costs in patients treated with aflibercept compared to ranibizumab: new real-life evidence from Switzerland. *BMC Ophthalmol.* **17**, 234 (2017).
51. Dugel, P. U. *et al.* HAWK and HARRIER: Phase 3, Multicenter, Randomized, Double-Masked Trials of Brolucizumab for Neovascular Age-Related Macular Degeneration. *Ophthalmology* **127**, 72–84 (2020).
52. Rohm, M. *et al.* Predicting Visual Acuity by Using Machine Learning in Patients Treated for Neovascular Age-Related Macular Degeneration. *Ophthalmology* **125**, 1028–1036 (2018).
53. von der Burchard, C. *et al.* Retinal volume change is a reliable OCT biomarker for disease activity in neovascular AMD. *Graefes Arch. Clin. Exp. Ophthalmol.* **256**, 1623–1629 (2018).

FIGURE Legend

Figure 1. (a) Exemplar results of the automatic segmentation algorithm from a patient with choroidal neovascularization from age-related macular degeneration with resultant fibrovascular pigment epithelium detachment and subretinal fluid. A two-dimensional slice was selected an OCT scanning stack (left panel) with resultant automated segmentation overlap (middle and right panels). Each distinct outlined structures are extrapolated to volumetric measurements (i.e. cubic millimeters and microliters). **(b)** Schematic of the variables considered in this study. Visual acuity (VA) and quantitative optical coherence tomography (qOCT) parameters were assessed immediately prior to receiving anti-VEGF treatment. A cross-sectional correlation between qOCT values and VA acquired at the same time-points was evaluated (red). The value of qOCT parameters in predicting VA measured at future time-points were also considered (blue). Here, the anatomical treatment response following injections were included as additional independent variables. For instance, the anatomical treatment-response to treatment 2 would be the qOCT parameters measured after injection (qOCT $^{n+2}$) minus that measured before injection (qOCT $^{n+1}$). These independent variables were also used to model the incremental change in VA resulting from the next upcoming treatment (green).

Figure 2. Visual function and qOCT parameters during anti-VEGF treatment period. (a) Mean visual acuity (VA; early treatment diabetic retinopathy study [ETDRS] letters) and automatically segmented volumes (cubic microns or µl) of intraretinal fluid (IRF), subretinal fluid (SRF), subretinal hyperreflective material (SHRM), intraretinal hyperreflective foci (HRF), and pigment epithelial detachment (PED) from 6x6mm OCT scans at baseline (i.e. prior to starting treatment) and 1, 2, 3 and 12 months post-baseline. **(b)** Mean and **(c)** distribution (box plots and histogram) of incremental change in VA and retinal structure volumes following the first 3 injections in the induction phase. Error bars signify 95% confidence intervals.

Figure 3. Non-linear logistic regression predicting visual acuity. Visual acuity (VA) thresholds $\geq$ 70 and $\leq$ 35 ETDRS (early treatment diabetic retinopathy study) lettersat **(a)** 3 months and **(b)** 12 months after starting anti-VEGF therapy were evaluated. The predictive value of qOCT biomarkers at baseline was considered on their own (blue), but also in combination with baseline VA (green) and with incremental change in VA and qOCT biomarkers for each of the preceding induction injections (black). Area under the curve (AUC) is presented with 95% confidence intervals.

Supplementary Figure 1. Patient flow diagram of the Moorfields Eye Hospital (MEH) patients with neovascular age-related macular degeneration (AMD)

Figure 1

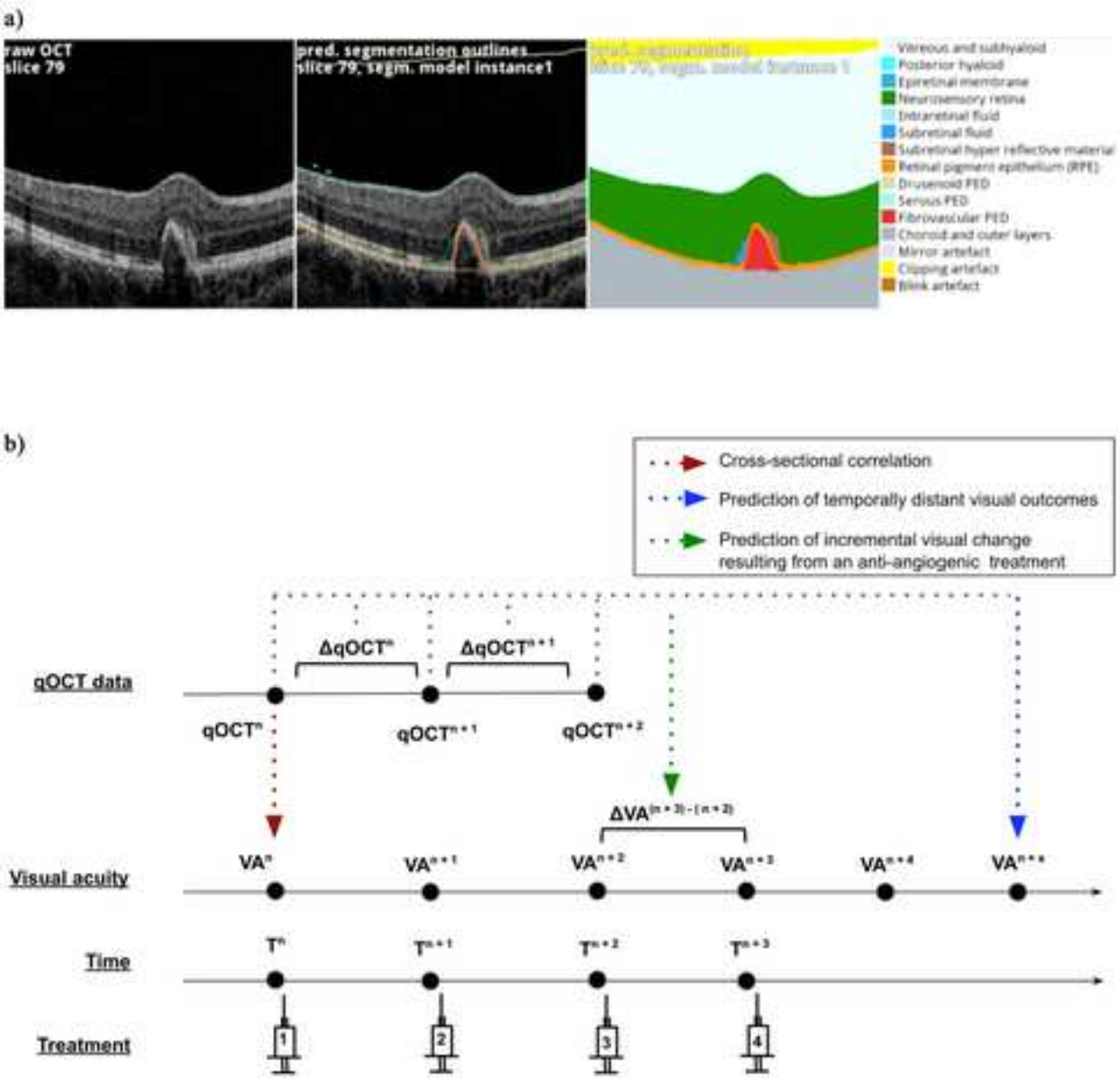

Figure 2

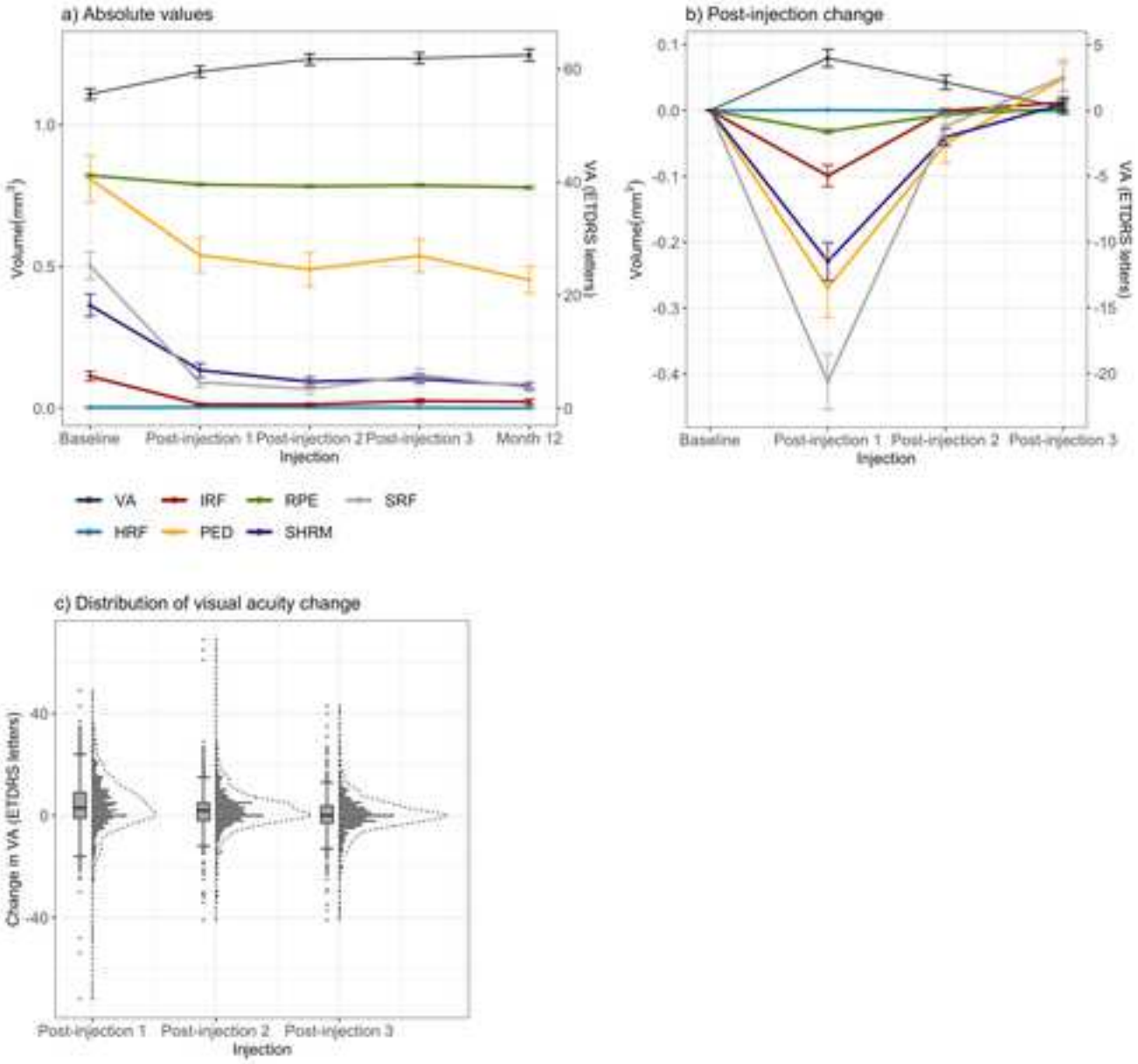

Figure 3

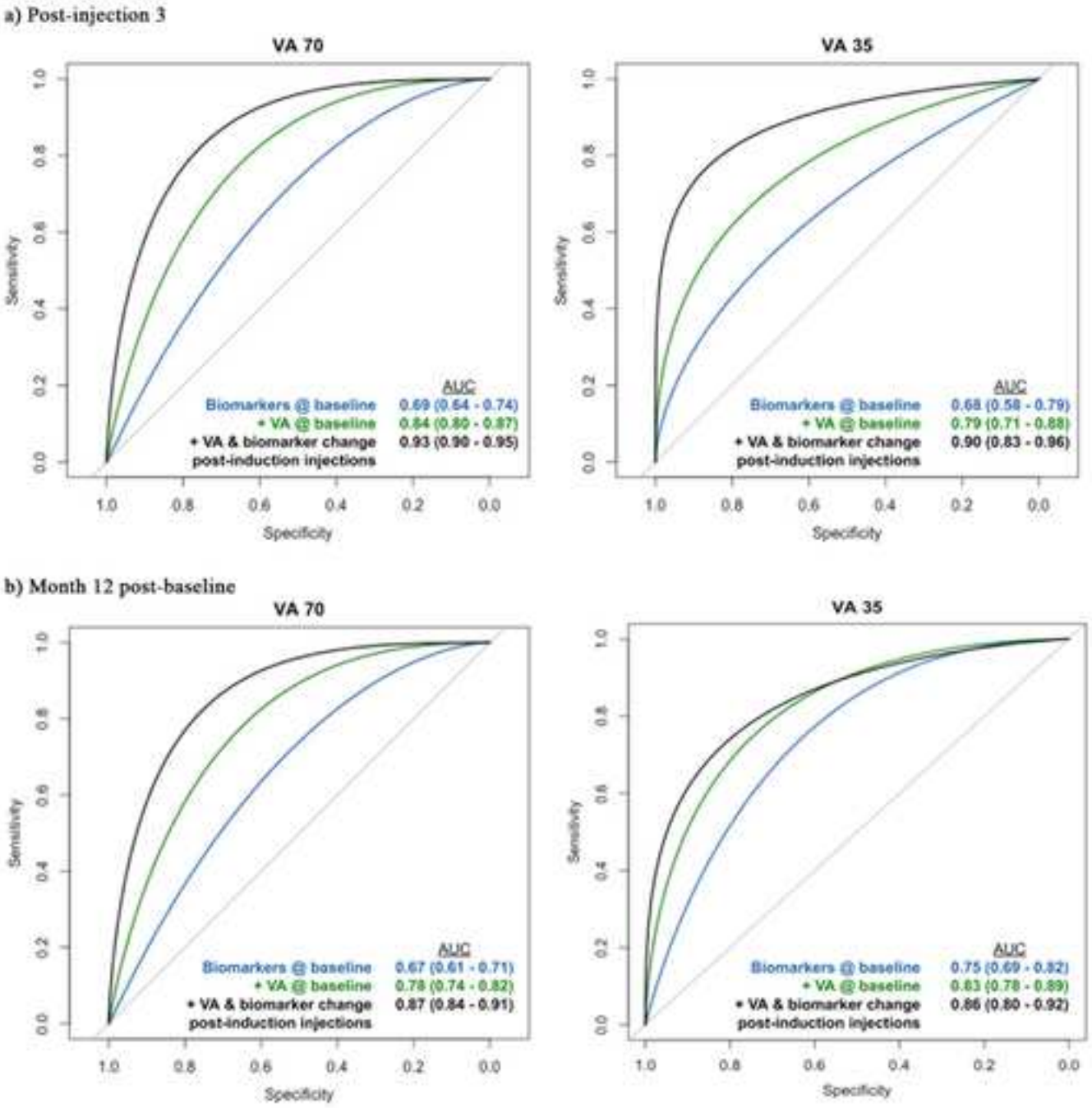

Table 1. Demographics and clinical features of cohort. Means, standard deviations (SD), distributions, and proportions are shown for **(a)** gender, ethnicity, baseline age, and whether the eye taken forward for analysis was the first-treated eye or one of simultaneously-treated eyes; and (**b**) clinical features i.e. visual acuity (VA; ETDRS [early treatment diabetic retinopathy study] letters]) and VA change from baseline was considered at baseline, post-injection 1, post-injection 2, post-injection 3, and at 12 months post-baseline. Baseline central retinal thickness (CRT) and change in CRT from baseline was similarly extrapolated. Baseline was considered as the timepoint immediately preceding initiation of anti-VEGF therapy.

Table 1a Demographics

	Overall (n=926)
Age (years)	
Mean (SD)	78.9 (8.68)
Median [Min, Max]	80.0 [49.0, 100]
Ethnicity	
Afro Caribbean	24 (2.6%)
Asian	92 (9.9%)
Caucasian	492 (53.1%)
Other	218 (23.5%)
Unknown	100 (10.8%)
Gender	
Female	541 (58.4%)
Male	385 (41.6%)
Treatment sequence	
First treated	880 (95.0%)
Simultaneously treated	46 (5.0%)

Table 1b Clinical features

	Baseline (n=926)	Post-injection 1	Post-injection 2	Post-injection 3	Month 12
VA (ETDRS letters)					
Mean (SD)	55.5 (15.0)	59.5 (15.4)	61.7 (15.1)	61.9 (15.3)	62.4 (16.5)
Median [Min, Max]	58.0 [0.00, 85.0]	62.0 [0.00, 95.0]	64.0 [0.00, 89.0]	65.0 [5.00, 90.0]	65.0 [2.00, 91.0]
VA ≥70 letters					
No	728 (78.6%)	657 (71.0%)	597 (64.5%)	581 (62.7%)	545 (58.9%)
Yes	198 (21.4%)	269 (29.0%)	329 (35.5%)	345 (37.3%)	381 (41.1%)
VA ≤35 letters					
No	797 (86.1%)	849 (91.7%)	865 (93.4%)	857 (92.5%)	843 (91.0%)
Yes	129 (13.9%)	77 (8.3%)	61 (6.6%)	69 (7.5%)	83 (9.0%)
VA change post-injection					
Mean (SD)	0.00 (0.00)	3.98 (10.4)	2.15 (8.38)	0.199 (7.36)	0.566 (10.0)
Median [Min, Max]	0.00 [0.00, 0.00]	3.00 [-72.0, 49.0]	2.00 [-41.0, 69.0]	0.00 [-41.0, 43.0]	1.00 [-53.0, 40.0]
VA change ≥ 5 letters					
No	926 (100%)	381 (41.1%)	523 (56.5%)	575 (62.1%)	395 (42.7%)
Yes	0 (0%)	545 (58.9%)	403 (43.5%)	351 (37.9%)	531 (57.3%)
VA change ≥ 10 letters					
No	926 (100%)	637 (68.8%)	771 (83.3%)	788 (85.1%)	672 (72.6%)
Yes	0 (0%)	289 (31.2%)	155 (16.7%)	138 (14.9%)	254 (27.4%)
CRT (μm^2)					
Mean (SD)	354 (114)	259 (73.2)	249 (67.1)	259 (73.7)	245 (63.7)
Median [Min, Max]	332 [0.0550, 995]	246 [0.00, 667]	237 [76.0, 593]	245 [95.1, 678]	237 [84.0, 674]
CRT change post-injection					
Mean (SD)	0.00 (0.00)	-94.4 (98.2)	-10.5 (53.3)	10.3 (54.3)	-14.3 (63.9)
Median [Min, Max]	0.00 [0.00, 0.00]	-77.3 [-563, 336]	-6.07 [-324, 347]	2.95 [-329, 318]	-7.02 [-328, 322]

Table 2. Structure-function correlation between visual acuity and qOCT biomarkers. Adjusted regression coefficients of models at baseline (immediately prior to starting anti-VEGF therapy) and post-injection 1, post-injection 2, post-injection 3, and 12-months post-baseline are displayed. Linear regression model bootstrapped 100-fold.

Table 2.

Timepoint	R^2	RMSE	MAE	P-value
Baseline	0.16	13.8	11.0	< 0.001
Month 1	0.11	14.6	11.4	< 0.001
Month 2	0.11	14.3	11.4	< 0.001
Month 3	0.14	14.3	11.5	< 0.001
Month 12	0.17	15.2	11.9	< 0.001

Table 3. Multi-linear regression for visual acuity following injection 2, injection 3, and 12 months following start of anti-VEGF. Adjusted regression coefficients of the different models displayed to illustrate incremental benefit by inclusion of both visual acuity and OCT segmentation data at baseline and during induction phase. Linear regression model bootstrapped 100-fold.

Table 3.

	Post-injection 2				Post-injection 3				Month 12			
	R^2	**RMSE**	**MAE**	**P-value**	**R^2**	**RMSE**	**MAE**	**P-value**	**R^2**	**RMSE**	**MAE**	**P-value**
Model 1 OCT biomarkers @ baseline	0.15	14.1	11.3	< 0.001	0.16	14.1	11.2	< 0.001	0.14	15.3	12.1	< 0.001
Model 2 VA @ baseline	0.52	10.6	8.0	< 0.001	0.47	11.2	8.5	< 0.001	0.34	13.4	10.2	< 0.001
Model 3 OCT biomarkers @ baseline + VA @ baseline	0.53	10.5	8.0	< 0.001	0.49	11.0	8.4	< 0.001	0.36	13.2	9.9	< 0.001
Model 4 OCT biomarkers @ baseline + VA @ baseline + VA & OCT changes post-injection	0.72	7.9	5.5	< 0.001	0.79	7.2	5.0	< 0.001	0.63	10.1	7.2	< 0.001

Table 4. Incremental VA change from an anti-VEGF treatment. VA change resulting from second and third anti-VEGF injection was queried. Adjusted regression coefficients of the different models displayed to illustrate incremental benefit by inclusion of both visual acuity and OCT segmentation data at baseline and during induction phase. Linear regression model bootstrapped 100-fold.

Table 4. Incremental VA change from an anti-VEGF treatment

	Post-injection 2				Post-injection 3			
	R^2	**RMSE**	**MAE**	**P-value**	**R^2**	**RMSE**	**MAE**	**P-value**
Model 1 OCT biomarkers @ baseline	0.002	8.5	5.5	0.07	0.002	7.6	5.1	0.85
Model 2 VA @ baseline	0.01	8.3	5.5	< 0.01	0.002	7.3	5.0	0.32
Model 3 OCT biomarkers @ baseline + VA @ baseline	0.01	8.3	5.6	< 0.001	0.002	7.7	5.1	0.67
Model 4 OCT biomarkers @ baseline + VA @ baseline + VA & OCT changes post-injection	0.13	8.1	5.6	< 0.001	0.07	7.3	5.0	< 0.01

Supplementary Figure 1

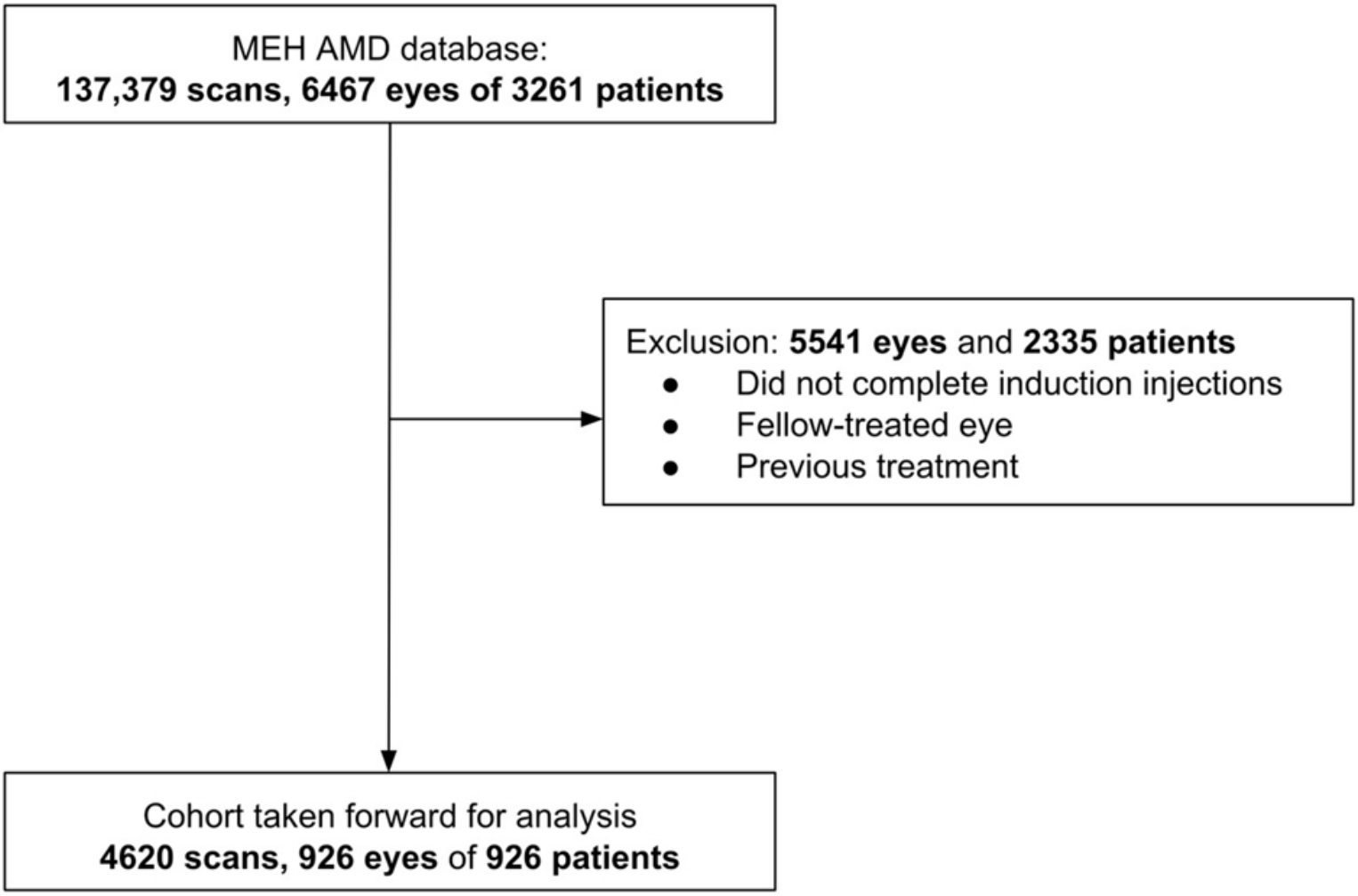

Supplementary Table 1. Mean visual acuity and retinal tissue volumes over the 12 month observation period. (a) Mean visual acuity (VA) in ETDRS (early treatment diabetic retinopathy study) letters at baseline, post-injection 1, post-injection 2, post-injection 3, and at 12 months post-baseline. **(b)** Mean retinal tissue volumes (cubic microns) of intraretinal fluid (IRF), subretinal fluid (SRF), subretinal hyperreflective material (SHRM), intraretinal hyperreflective foci (HRF), and pigment epithelial detachment (PED) segmented automatically from 6x6mm OCT scans. Mean change in **(c)** VA and **(d)** retinal volumes from baseline post-injection 1, post-injection 2, and post-injection 3. Each mean is displayed with 95% confidence intervals.

a) Mean visual acuity			**b) Mean retinal tissue volumes (mm^3)**											
Timepoint	VA	95% CI	HRF	95% CI	IRF	95% CI	PED	95% CI	RPE	95% CI	SHRM	95% CI	SRF	95% CI
Baseline	55.55	0.97	0.003	0.001	0.113	0.017	0.809	0.082	0.821	0.005	0.364	0.039	0.503	0.048
Post-injection 1	59.53	0.99	0.004	0.001	0.014	0.004	0.540	0.061	0.789	0.005	0.134	0.024	0.092	0.016
Post-injection 2	61.68	0.97	0.003	0.001	0.014	0.005	0.490	0.059	0.783	0.005	0.094	0.016	0.068	0.018
Post-injection 3	61.88	0.99	0.002	0.000	0.026	0.008	0.538	0.058	0.787	0.005	0.104	0.015	0.118	0.022
Month 12	62.45	1.07	0.001	0.000	0.022	0.010	0.452	0.047	0.779	0.005	0.080	0.012	0.074	0.016

c) Mean change in visual acuity			**d) Mean change in retinal tissue volumes (mm^3)**											
Timepoint	VA	95% CI	HRF	95% CI	IRF	95% CI	PED	95% CI	RPE	95% CI	SHRM	95% CI	SRF	95% CI
Post-injection 1	3.98	0.67	6.5E-04	3.7E-04	-0.10	0.02	-0.27	0.05	-0.03	3.4E-03	-0.23	0.03	-0.41	0.04
Post-injection 2	2.15	0.54	-2.8E-04	2.3E-04	-5.9E-04	3.2E-03	-0.05	0.03	-0.01	2.7E-03	-0.04	0.01	-0.02	0.02
Post-injection 3	0.20	0.47	-1.0E-03	2.9E-04	0.01	0.01	0.05	0.03	3.2E-03	2.9E-03	0.01	0.01	0.05	0.02

Supplementary Table 2. Correlation between qOCT parameters and cross-sectional visual acuity (VA). Adjusted regression coefficients of models at baseline (immediately prior to starting anti-VEGF therapy) and post-injection 1, post-injection 2, post-injection 3, and 12-months post-baseline. Variables were automatically-segmented retinal structures: intraretinal fluid (IRF), subretinal fluid (SRF), subretinal hyperreflective material (SHRM), intraretinal hyperreflective foci (HRF), and pigment epithelial detachment (PED). Linear regression model bootstrapped 100-fold.

Baseline					**Post-injection 1**				
	Coefficient	Standard error	T-value	P-value		Coefficient	Standard error	T-value	P-value
SHRM	-6.98	0.80	-8.77	< 0.001	**RPE**	45.83	6.54	7.01	< 0.001
IRF	-12.58	1.74	-7.24	< 0.001	**SHRM**	-9.20	1.38	-6.64	< 0.001
RPE	33.89	6.73	5.03	< 0.001	**IRF**	-21.29	7.13	-2.98	< 0.001
SRF	-1.56	0.66	-2.36	0.02	**PED**	-1.29	0.55	-2.33	0.02
HRF	-113.51	59.87	-1.90	0.06	**HRF**	-92.20	48.95	-1.88	0.06
PED	-0.31	0.39	-0.81	0.42	**SRF**	1.89	2.13	0.89	0.37

Post-injection 2					**Post-injection 3**				
	Coefficient	Standard error	T-value	P-value		Coefficient	Standard error	T-value	P-value
RPE	46.21	5.97	7.73	< 0.001	**RPE**	52.04	5.93	8.78	< 0.001
SHRM	-11.42	2.02	-5.66	< 0.001	**SHRM**	-12.94	2.17	-5.97	< 0.001
HRF	-154.84	50.30	-3.08	< 0.001	**IRF**	-14.96	3.82	-3.92	< 0.001
IRF	-16.28	6.17	-2.64	0.01	**PED**	-1.66	0.59	-2.79	0.01
PED	-1.38	0.56	-2.48	0.01	**HRF**	-198.84	72.12	-2.76	0.01
SRF	-1.29	1.77	-0.73	0.47	**SRF**	0.94	1.51	0.62	0.53

12 months post-baseline				
	Coefficient	Standard error	T-value	P-value
RPE	56.20	6.02	9.33	< 0.001
SHRM	-22.46	2.89	-7.78	< 0.001
IRF	-13.25	3.16	-4.19	< 0.001
PED	-1.17	0.76	-1.54	0.12
SRF	2.69	2.18	1.23	0.22
HRF	-0.68	227.45	0.00	1.00

Supplementary Table 3. Predictive covariates of incremental visual change resulting from injection 2 and 3. Adjusted regression coefficients of covariates in a model of visual acuity change resulting from injection 2 and injection 3. Variables included visual acuity (VA) and automatically-segmented retinal structures (intraretinal fluid [IRF], subretinal fluid [SRF], subretinal hyperreflective material [SHRM], intraretinal hyperreflective foci [HRF], and pigment epithelial detachment [PED]) at baseline and changes resulting from previous injections. Linear regression model bootstrapped 100-fold.

Post-injection 2					**Post-injection 3**				
	Coefficient	Standard error	T-value	P-value		Coefficient	Standard error	T-value	P-value
VA (Baseline)	0.84	0.02	41.81	< 0.001	VA (Baseline)	0.91	0.02	48.86	< 0.001
VA change (Post-injection 1)	0.69	0.03	25.96	< 0.001	VA change (Post-injection 1)	0.86	0.03	33.52	< 0.001
RPE change (Post-injection 1)	13.34	5.49	2.43	0.02	VA change (Post-injection 2)	0.69	0.03	23.19	< 0.001
IRF (Baseline)	-6.16	3.91	-1.58	0.12	IRF change (Post-injection 2)	-11.55	4.82	-2.40	0.02
PED (Baseline))	-0.33	0.22	-1.48	0.14	RPE change (Post-injection 1)	11.86	5.23	2.27	0.02
IRF change (Post-injection 1)	-5.87	4.11	-1.43	0.15	SHRM change (Post-injection 2)	-3.92	1.91	-2.06	0.04
RPE (Baseline)	5.76	4.06	1.42	0.16	PED change (Post-injection 1)	-2.22	1.28	-1.74	0.08
HRF change (Post-injection 1)	-99.91	73.69	-1.36	0.18	IRF (Baseline)	-6.06	3.56	-1.70	0.09
SRF change (Post-injection 1)	-1.64	1.32	-1.25	0.21	SRF (Baseline)	-1.76	1.14	-1.54	0.12
SHRM (Baseline)	-0.67	0.76	-0.88	0.38	RPE (Baseline)	5.56	3.64	1.53	0.13
HRF (Baseline)	-29.93	34.58	-0.87	0.39	SHRM (Baseline)	-1.64	1.08	-1.51	0.13
SHRM change (Post-injection 1)	0.43	0.98	0.44	0.66	IRF change (Post-injection 1)	-4.76	3.73	-1.27	0.20
SRF (Baseline)	-0.47	1.16	-0.40	0.69	PED (Baseline)	-0.19	0.20	-0.95	0.34
					HRF change (Post-injection 2)	-55.60	66.16	-0.84	0.40
					RPE change (Post-injection 1)	4.71	5.94	0.79	0.43
					SHRM change (Post-injection 1)	-0.96	1.23	-0.78	0.44
					SRF change (Post-injection 2)	0.46	0.98	0.47	0.64
					HRF (Baseline)	-4.61	30.99	-0.15	0.88